Earthquake Geotechnical Engineering for Protection and Development of Environment and Constructions – Silvestri & Moraci (Eds)
© 2019 Associazione Geotecnica Italiana, Rome, Italy, ISBN 978-0-367-14328-2

Characteristics of ocean-floor time series of shallow crustal earthquakes recorded by DONET in Japan

T. Kishida, R.L. Sousa, G.L. Zhu & Y.J. Byon
Khalifa University of Science and Technology, Abu Dhabi, UAE

Y. Sugiyama
Port and Airport Research Institute, Yokosuka, Japan

ABSTRACT: Many offshore structures are constructed at locations that are earthquake prone; therefore, their associated seismic designs are required. However, the selection of the acceleration time series for seismic design is difficult because recorded ground motions at the ocean-bottom seafloor are limited. Recently, the Japan Agency for Marine-Earth Science and Technology (JAMSTEC) installed the ocean-bottom seismology network (DONET) at the offshore of the Kii Peninsula in Japan. Twenty stations are recording three-component time series using accelerometers and seismometers. These time series are publicly available since 2012 at the JAMSTEC website (https://join-web.jamstec.go.jp/JSEIS/). This study selects representative time series of shallow crustal earthquakes and processes from DONET to develop a database of ocean-bottom ground motion. These time series are compared to the inland recordings from the Kyoshin network (K-NET). This study reviews the instrument responses of the accelerometers and seismograms of DONET. Fourier amplitude spectra (FAS) are also computed for different time windows, and the ocean floor and inland FAS are compared to understand the characteristics of ocean-floor recordings. Horizontal and vertical attenuations are also compared between ocean floor and inland and with the results of typical ground-motion prediction models. Finally, the horizontal-to-vertical spectral ratios (HVSRs) are computed for the ocean-floor stations to understand its local site effects.

1 OCEAN BOTTOM NETWORK FOR DONET

1.1 *Overview*

The Japan Agency for Marine-Earth Science and Technology (JAMSTEC) installed twenty ocean-bottom seismology (OBS) stations (DONET) at the offshore of Kii Peninsula in Japan. These sensors are used for real-time seismic monitoring to provide more accurate hypocenter locations and earthquake magnitude for subduction earthquakes. Moreover, these recordings will be useful for engineering practices as they provide more accurate information of ground motion for realistic designing of offshore structures such as oil platform and wind turbines. Since there are uncertainties in soil properties at the ocean floor, the seismic recordings will be also useful to estimate the site conditions (e.g. top 30-m averaged shear wave velocities (V_{s30})).

Figure 1 shows the station locations of DONET at the offshore of Kii Peninsula in Japan. Stations are located about 2,000 to 4,000 m below the sea level from the ocean-bottom to near subduction Nankai trough. Figure 2 shows a typical instrument response of seismometers and accelerometers of DONET. Nyquist frequencies of seismometers and accelerometers are 10 and 100 Hz, respectively. The seismometers responses are flat from 0.001 to 3 Hz showing the capability of measuring long-period signals. The responses of the accelerometers are also flat for entire frequency ranges. Table 1 lists the shallow crustal earthquakes considered in this study, including 2016 Kumamoto Earthquakes, 2016 **M**6.2 Tottori Earthquake, and 2018 **M**5.6 North Osaka

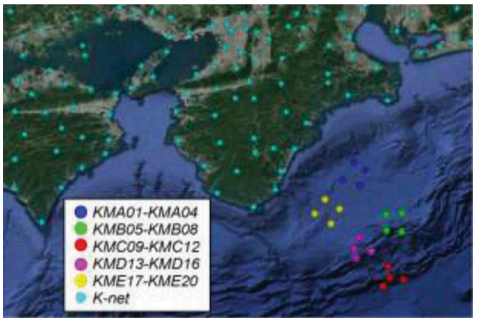

Figure 1. Location of DONET stations

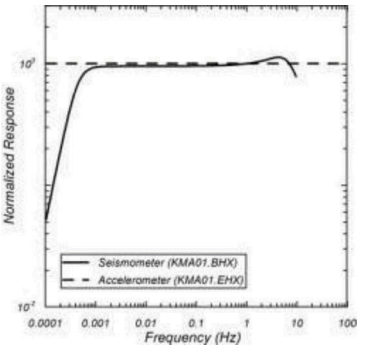

Figure 2. Typical instrument responses for seismometer and accelerometer in DONET

Earthquake. The moment magnitudes (**M**) range from 5.6 to 7.0 where the largest one is the 2016 Kumamoto Earthquake. In total, 91 3-component time series are included in the database by downloading the time series in "seed" format from DONET. These files are converted to ASCII files using the program of "rdseed" (https://ds.iris.edu/ds/nodes/dmc/manuals/rdseed/). Instrument corrections are applied only for seismometers before processing the time series. We prioritize the recordings by accelerometers over seismometers when hypocentral distances are less than 300 km. When the hypocenter distances are greater than 300 km, time series by seismometer were prioritized over accelerometers because of their capability to record the low-amplitude signals.

Available time series, recorded in land, corresponding to the events being studied were also downloaded from Kyoshin network (K-NET) (http://www.kyoshin.bosai.go.jp/). Shear wave velocity (V_s) profiles are available for these sites from National Research Institute for Earth Science and Disaster Resilience (NIED) website. These time series are also processed to develop the ground motion database. In total, more than 1,200 3-component time series were processed from K-NET.

1.2 *Ground motion processing*

The downloaded time series are processed by the strong motion data processing method in accordance with Pacific Earthquake Engineering Research Center (PEER) (Chiou et al. 2008, Ancheta et al. 2014, Kishida et al. 2016). Figures 3(a) and 3(b) show the processed horizontal time series of the 2018 **M**5.5 Osaka Earthquake at AIC009 from K-NET and at KMA001 from DONET, respectively. V_{s30} of AIC009 is calculated as 277 m/s (Boore et al. 2011) and classified as soft soils (i.e. $V_{s30} < 360$ m/s). V_{s30} of KMA001 is unknown but expected to be very soft. The hypocentral distances are about 140 km for both recordings. The figures show that the P-wave durations are about 17 sec for both records indicating that the hypocenter distances are approximately the same. Both records also show similar peak acceleration of 0.018g. However, there are clear differences between these records in durations and long-period amplitudes. The

Table 1. Shallow crustal earthquake catalog for ocean bottom seismograph for data processing

Earthquake ID	Origin Time (UTC)	Earthquake Name	**M**	Number of Record	
				DONET	K-net
1	2016-04-14T12:26:35	Kumamoto, FS	6.2	20	187
2	2016-04-14T15:03:47	Kumamoto, FS	6.0	20	160
3	2016-04-15T16:25:06	Kumamoto, MS	7.0	20	266
4	2016-10-21T05:07:23	Tottori	6.2	16	309
5	2018-06-17T22:58:35	North Osaka	5.6	15	298

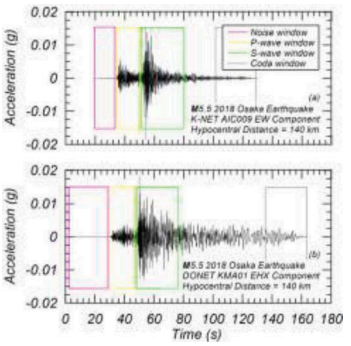

Figure 3. Comparison of processed time series between (a) K-NET AIC009 and (b) DONET KMA01

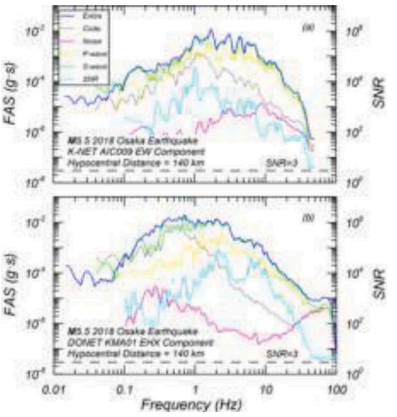

Figure 4. Comparison of unprocessed horizontal FAS between (a) K-NET AIC009 and (b) DONET KMA01

acceleration amplitudes are larger for ocean-floor recordings than those for inland ones after S-wave packets, which leads to the longer durations at the ocean-floor. Figures 4(a) and 4(b) show the Fourier Amplitude Spectra (FAS) of the windowed unprocessed time series where these P-, S-, Coda, and entire windows are presented in Figures 3(a) and 3(b). The windowing method follows the approach by Kishida et al. (2016). Figure 4 shows that the FASs are similar between ocean-bottom (i.e. DONET) and inland (i.e. K-net) for P-wave windows. However, the significant differences appear in the Coda window on the FAS amplitudes in which KMA001 has larger amplitudes from 0.3 to 0.6 Hz compared to AIC009. This indicates that the late-arriving surface waves with the period of 1.7 to 3.3 s have the larger amplitude at the ocean-bottom than inland. Boore (1999a) observed a similar trend at 1990 Upland earthquakes and explained that these larger amplitudes with the period greater than a few seconds are explained by the surface waves generated from Los Angeles basin. Figures 5(a) and 5(b) show the processed time series in vertical directions at the same stations. It is observed that the body-wave amplitudes (i.e. P-, and S-wave) are lower at the ocean-floor compared to the inland, even though these stations observed the similar acceleration amplitude in horizontal directions (i.e. Figure 3). This observation could be related to the influence of water pressures at the ocean-floor (e.g. Boore and and Smith 1999); but it is believed that further detailed analyses are required by considering these resonance frequencies. The wave amplitude becomes larger after S-wave window at the ocean floor in Figure 3(b), indicating that these are clearly contributed by surface waves than the body waves. Figures 6(a) and 6(b) show the FAS of the vertical time series in Figures 5(a) and 5(b). The peaks of FAS appear around 1.5 Hz at AIC009 in the S-wave window, where these peaks are appeared around 0.4 Hz at KMA001 in Coda window. These observations indicate that the surface waves are important characteristics for horizontal and vertical time series at the ocean-floor which might not be considered in offshore-structure design practices by using the inland recordings. Differences in the ground motion attenuation between ocean floor and inland are further discussed in the following section.

2 GROUND MOTION ATTENUATION

2.1 *Horizontal ground motion attenuation*

Figure 7 shows the ground motion attenuations of horizontal spectral accelerations (PSA) of RotD50 (Boore 2010) at the period of 0.2, and 3.0 s with the closest distance. Figures 7a-7b, 7c-7d, and 7e-7f show the data from 2016 **M**7.0 Kumamoto, 2016 **M**6.2 Tottori, and 2018 **M**5.6 North Osaka Earthquake, respectively. Site conditions are classified as "Rock", "Stiff", and "Soft" for K-net based on V_{s30} (i.e. Rock: $V_{s30} > 760$ m/s, Stiff: $360 < V_{s30} < 760$ m/s, Soft: $V_{s30} < 360$ m/s) and "ocean floor" for DONET, respectively. The figure shows that the PSA at

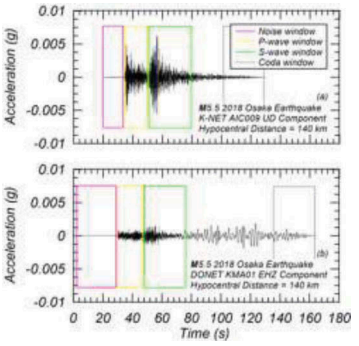

Figure 5. Comparison of processed vertical time series between (a) K-NET AIC009 and (b) DONET KMA01

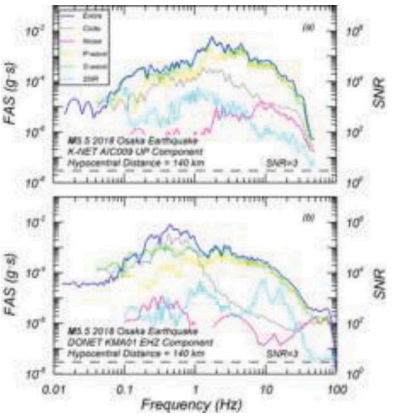

Figure 6. Comparison of unprocessed vertical FAS between (a) K-NET AIC009 and (b) DONET KMA01

T = 0.2 s at the ocean-floor is reasonably consistent with other site conditions for all earthquakes. However, at T = 3.0 s, the PSAs at ocean floor are significantly higher than the other site conditions, especially for 2018 **M**5.6 North Osaka Earthquake. It is noted that Osaka is located at one of the largest urban basins in Japan. The figures also show the average of predicted values with V_{s30} = 360 m/s by NGA-West2 ground motion models (GMMs) (Abrahamson et al. 2014, Campbell and Bozorgnia 2014, Boore et al. 2014, Chiou and Youngs 2014). The

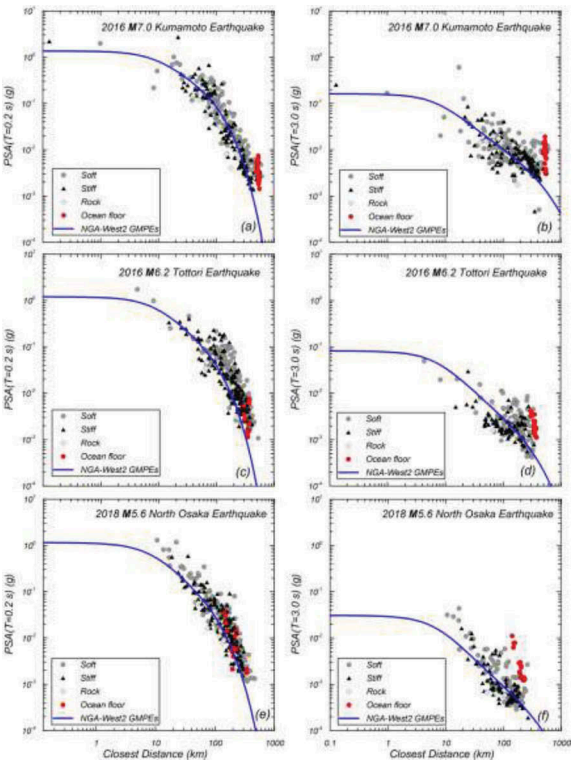

Figure 7. Horizontal PSA vs. closest distances at 0.2 and 3.0 s for different earthquakes

comparison shows reasonable agreement of predicted values to the observations. However, the consistent underestimations of PSA at 3.0 s at the ocean-floor are prominent by using shallow crustal GMMs. Therefore, some adjustments are required for surface waves on GMMs when seismic designs are performed against shallow crustal earthquakes for offshore structures.

2.2 *Vertical ground motion attenuation*

Figure 8 shows the vertical PSA at the period of 0.2, and 3.0 s with closest distance. The PSA at T = 0.2 s at ocean floor reasonably consistent with inland records for all earthquakes even though the mean values seem to be lower than the average of inland recordings compared to the data in Figure 7. However, at T = 3.0 s, the PSA at ocean floor are clearly higher than the inland records, especially for 2018 **M**5.6 North Osaka Earthquake. For example, Figure 8f shows that the closest distances are about 200 km for ocean floor recordings. However, these amplitudes approximately correspond to those at 20-30 km for inland recordings. Therefore, the influence of surface waves is very large at ocean floor for vertical ground motions. The blue lines in Figures 8a-8f show the predicted vertical PSA by Bozorgnia and Campbell (2016) with V_{s30} = 360 m/s. The comparison between the predicted and the recorded PSA shows reasonable agreement at inland for the periods at 0.2 s and 3.0 s, even though more detailed analyses are required to evaluate the GMM with event terms and path effects. However, for ocean-floor PSA, we can clearly observe that the shallow crustal GMMs underestimate the effects of surface waves from the period of 2.0 to 5.0 s when seismic designs are performed for offshore structures.

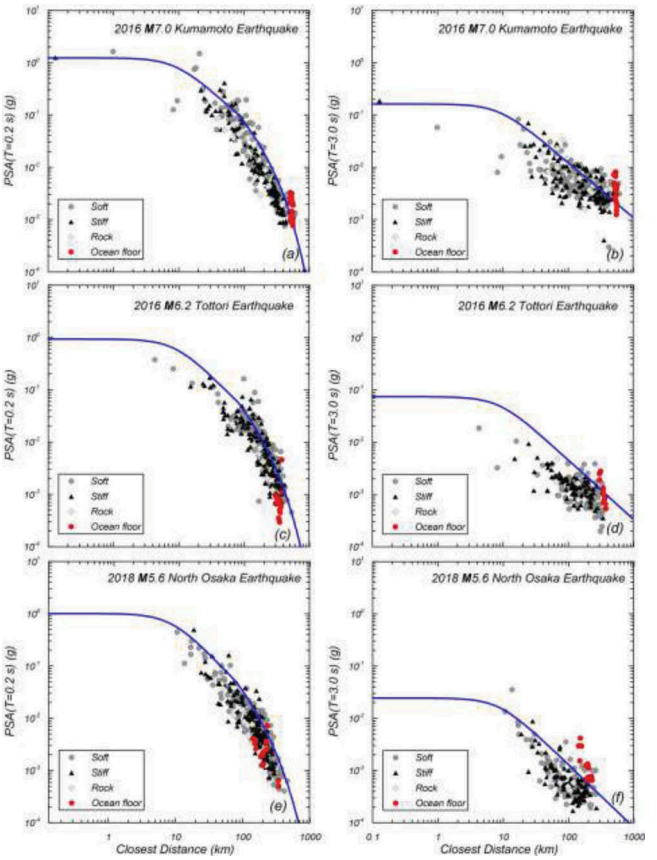

Figure 8. Vertical PSA vs. closest distances to the fault at 0.2 and 3.0 s for different earthquakes

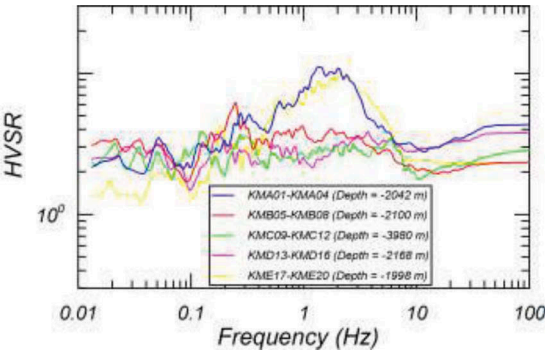

Figure 9. HVSR for different station locations

2.3 *Horizontal-to-Vertical Spectral Ratio (HVSR)*

Figure 9 shows the HVSR at different station locations obtained from the downloaded unprocessed time series. The HVSR are often used to understand the S-wave amplification in horizontal components with respect to bedrock (Nakamura 1989). It shows that HVSR for KMA01-KMA04 and KME17-KME20 are very similar with clear peaks at the frequency of 1.3 to 2.0 Hz. These stations exist closer to land when compared to other stations (Figure 1). The peaks of HVSR for KMB05-KMB08, KMC09-KMC12, and KMD13-KMD16 are around 0.2 Hz which is lower than KMA01-KMA04 and KME17-KME20. These sites locate near the subduction Nankai trough (Figure 1). These changes may relate to the thickness of soft soil deposits and impedance contrast between bedrock and subsurface deposits. These observations show that body-wave amplifications will be large near the land rather than the sites which are closer to the subduction Nankai trough. However, none of these HVSR show a clear peak at the frequency of 0.4 Hz as observed in FAS in Figures 4 and 6. Since peak frequencies of FAS in Figures 4 and 6 are different from those of HVSR in Figure 9, the large amplitudes at 0.4 Hz observed in ocean-floor recordings are not related to the local site effects. This observation is consistent with those in Figures 4 and 6 where the large amplitude of FAS around 0.4 Hz is contributed by the surface waves after S-wave packets.

3 CONCLUSION

This study downloaded the time series of shallow crustal earthquakes by DONET operated by JAMSTECS. These stations are located at the ocean-floor near the offshore of Kii Peninsula. Instrument responses are reviewed for these time series and processed by following the standard data processing method by PEER. Time series from K-NET by NIED, from stations located in land, were also downloaded and processed. The time series from ocean-floor and inland are compared in time domain by windowing the time series into different wave packets. The comparison shows that the time series measured at the ocean-floor have significantly large amplitudes in Coda window after S-wave packets, while these characteristics are not observed in the times series recorded inland. The ocean floor and inland FAS are also compared. The comparison shows that the inland peak FAS occurs at the frequency of 1.5 Hz in S-wave window, while the ocean floor peak FAS occurs at the frequency of 0.4 Hz in Coda window. These observations show that the large amplitudes in Coda window at ocean floor are contributed by surface waves, which might be generated at the edge of the basin in the land through wave propagations.

The attenuation of PSA at 0.2 and 3.0 s are reviewed against the closest distances to the faults for ocean-floor and inland recordings for horizontal and vertical components. The GMMs are compared to these observations. The comparison shows that PSA at 0.2 s are reasonably consistent for ocean-floor recordings with GMMs even though uncertainties exist for

V_{s30} and influence of underwater for ocean-floor recordings in vertical direction. However, for PSA at 3.0 s, the amplitudes are clearly higher at the ocean floor recordings than in the inland recordings and the GMMs for horizontal and vertical components. These differences are due to the surface waves at ocean floor generated through wave propagations.

The HVSR are also reviewed for ocean floor recordings. The results show that the clear peak responses are observed around 1.5 Hz when the station is located at ocean bottom near the land. When the stations are located near the subduction Nankai trough, the peak responses become unclear. These peak frequencies in HVSR do not match to the frequencies at which the peak amplitude of FAS are observed for ocean-floor recordings (i.e. around 0.4 Hz). This indicates that the peak amplitudes at ocean-floor do not result from the S-wave amplification due to the local site effects, but from the surface waves.

Based on the observations from the windowed FAS amplitudes, PSA attenuations, and HVSR, we can conclude that the surface waves have significant amplitude at ocean floor for shallow crustal earthquakes. These characteristics cannot be captured in design practices of offshore structures when using the time series and GMMs based on inland observations. Therefore, the seismic design of offshore oil platform and wind turbine requires that one specifically takes in consideration the effect of these surface waves. Otherwise structural design becomes unsafe for resonance responses and cyclic loading due to the surface waves generated through wave propagations at inland basin edges.

REFERENCES

Abrahamson, N. A., Silva, W. J., and Kamai, R., 2014. Summary of the Abrahamson, Silva, and Kamai NGA-West2 ground-motion relations for active crustal regions, Earthquake Spectra 30, 1025–1055.

Ancheta, T. D., Darragh, R. B., Stewart, J. P., Seyhan, E., Silva, W. J., Chiou, B. S., Wooddell, K. E., Graves, R. W., Kottke, A. R., Boore, D. M., Kishida, T., and Donahue, J. L., 2014. NGA-West 2 database, *Earthquake Spectra* 30, 989–1005.

Boore D.M., Thompson E.M., Cadet H. (2011). Regional correlations of VS30 and velocities averaged over depths less than and greater than 30 m, Bull. Seismol. Soc. Am., 101(6): 3046–3059.

Boore D.M. (1999a). Basin waves on a seafloor recording of the 1990 Upland, California, earthquake: Implications for ground motions from a larger earthquake, Bull. Seism. Soc. Am. 89, 317–324.

Boore D.M. and Smith C. E. (1999b). Analysis of earthquake recordings obtained from the seafloor earthquake measurement system (SEMS) instruments deployed off the coast of southern California, *Bull. Seism. Soc. Am*. 89, 260–274.

Boore D.M., (2010). Orientation-Independent, Nongeometric-Mean Measures of Seismic Intensity from Two Horizontal Components of Motion, *Bulletin of the Seismological Society of America*, 100, No. 4, pp. 1830–1835, August 2010, doi: 10.1785/0120090400.

Boore D.M., Stewart, J. P. and Seyhan, E. and Atkinson, G. M. (2014), NGA-West2 Equations for Predicting PGA, PGV, and 5-% Damped PSA for Shallow Crustal Earthquakes, Earthquake Spectra, 30, 3, 1057–1085, doi = 10.1193/070113EQS184M.

Bozorgnia Y., Campbell K.W. (2016). Vertical Ground Motion Model for PGA, PGV, and Linear Response Spectra Using the NGA-West2 Database. Earthquake Spectra: May 2016, Vol. 32, No. 2, pp.979–1004.

Campbell, K. W., and Bozorgnia, Y., 2014. NGA-West2 ground motion model for the average horizontal components of PGA, PGV, and 5%-damped linear Response Spectra, Earthquake Spectra 30, 1087–1115.

Chiou, B. S.-J., and Youngs, R. R. (2014). Update of the Chiou and Youngs NGA ground motion model for average horizontal component of peak ground motion and response spectra, Earthquake Spectra 30, 1117–1153.

Chiou, B., Darragh, R., Gregor, N., and Silva, W., 2008. NGA Project Strong-Motion Database, *Earthquake Spectra* 24, 23–44.

Kishida, T., Ktenidou, O.-J., Darragh, R. B. and Silva, W. J. (2016), "Semi-Automated Procedure for Windowing Time Series and Computing Fourier Amplitude Spectra for the NGA-West2 Database", Pacific Earthquake Engineering Research Center, PEER Report 2016/02.

Nakamura, Y. (1989). A method for dynamic characteristics estimation of subsurface using microtremor on the ground surface, Q. Rep. Railway Tech. Res. Inst. 30, 25–33.